Article:

Liu, Y., Huang, S.-S. orcid.org/0000-0003-2816-7104 and Burgess, I. orcid.org/0000-0001-9348-2915 (2021) Fire performance of axially ductile connections in composite construction. Fire Safety Journal, 121. 103311. ISSN 0379-7112

https://doi.org/10.1016/j.firesaf.2021.103311

Fire performance of axially ductile connections in composite construction

Yu Liu[1*], Shan-Shan Huang[1] and Ian Burgess[1]

[1] Department of Civil and Structural Engineering, University of Sheffield, Mappin Street, Sheffield S1 3JD, United Kingdom.

* Corresponding Author: E-mail address: yliu230@sheffield.ac.uk (Yu Liu)

Abstract

To enhance the robustness of steel-framed structures in fire, a novel, axially ductile connection has previously been proposed. In this paper its performance is investigated when it is used to connect composite beams to steel columns in composite steel-concrete construction. The ductile connection is designed to satisfy the ductility demands of the composite beam at elevated temperatures. A reinforcement component has been added to the bare-steel ductile connection model to establish a component-based model of the composite ductile connection. The connection model has been incorporated into the software Vulcan, and is validated against detailed Abaqus FE models using solid elements. Results show that the proposed component-based model can efficiently represent the behaviour of the connection given by the detailed Abaqus simulations. Parametric studies using Vulcan have been carried out, varying three parameters; the connection thickness, the semi-cylindrical section radius, and the density of longitudinal reinforcing bars. Finally, a 2-D Abaqus composite frame model has been created to investigate the influence of shear studs on the behaviour of the composite ductile connections under different stud spacings.

Keywords: Composite connection, Fire, Ductility demand, Component-based model

Notation list

Δ_r	Axial ductility demand of the beam at the rebar level
Δ_{cts}	Axial ductility demand of the beam at the connection top surface
Δ_{cbs}	Axial ductility demand of the beam at the connection bottom surface
Δ_{bbf}	Axial ductility demand of the beam at the beam bottom flange
θ_{total}	Total rotation of the composite beam at beam end
δ_{total}	Total deflection of the composite beam, $\delta_{total} = \delta_{external-load} + \delta_{thermal-bowing}$

l	The length of the composite beam
h_1	Slab depth
h_2	Steel beam depth
H_{con}	Connection depth
h_c	The vertical distance from the top surface of the slab to the neutral axis
h_r	The vertical distance from the top surface of the slab to the longitudinal rebar
T_{slab}	The tensile force acting at the centroid of the slab
C_{steel}	The compressive force acting at the centroid of the steel section
E_1	The Young's modulus of the slab
A_1	The cross-section area of the slab
I_1	The second moment of area of the slab
E_2	The Young's modulus of the steel section
A_2	The cross-section area of the steel section
I_2	The second moment of area of the steel section
α	Thermal expansion coefficient
e_1	The vertical distance from the neutral axis to the centroid of the slab
e_2	The vertical distance from the neutral axis to the centroid of the steel section
Def	The deflection due to thermal bowing
u_b	The bond stress when the rebar strain is lower than the yield strain
u_b'	The bond stress when the rebar strain is higher than the yield strain
l_d	The development length of elastic zone
l_d'	The development length of post-yield zone
d_b	The diameter of the rebar
f_y	The yield stress of rebar
ε_y	The yield strain of rebar
f_u	The ultimate stress of rebar
ε_u	The ultimate strain of rebar
f_s	Stress between f_y and f_u
f_c	Concrete strength
s_b	The regular spacing of the weld points on the transverse rebars

1. Introduction

Failure of the connections of a composite floor in fire conditions may lead to the detachment of connected beams, causing the collapse of floors, spread of fire into other compartments, buckling of the adjacent columns and may even initiate the eventual collapse of the entire building. Therefore, connection performance has a crucial influence on the control of the fire-induced progressive collapse of a composite structure. The behaviour of connections at elevated temperatures is considerably more complex than that at ambient temperature, since the connections undergo different combinations of loads at different stages of a fire event. In the initial stage, the major forces carried by connections are vertical shear, accompanied by some moment, depending on the type of connection. With the increase of temperature, connections can experience additional compressive force due to the restrained thermal expansion of the connected beam. This compressive force may eventually change to tension at very high temperatures when the connected beam is under catenary action due to highly reduced steel strength. It is therefore very difficult to reproduce such complex loading conditions in experiments except in full-scale structural fire tests [1]. In addition, due to the large variety of connection types and dimensions, a large number of experiments would be required to cover the investigation of a representative range of different connections. Hence, numerical simulation is the feasible alternative to study the performance of connections under fire conditions. This may consist of detailed finite element simulations or more global numerical analyses representing connections using a component-based method. Among these, the component-based method can be a good compromise between accuracy of results and computational cost, compared with detailed finite element modelling. This method, which was initially developed for the design of semi-rigid joints at ambient temperature, based on principles initially proposed by Zoetemeijer [2], has been introduced into Eurocode 3 Part 1-8 [3]. When creating the component-based model, the connection is divided into components representing basic zones of structural action, and each component is idealized as a nonlinear spring of known stiffness and strength.

Compared with bare-steel framing, composite construction has higher structural efficiency and lower cost, because it allows the use of smaller steel sections. Therefore, in recent decades, composite structures have been widely used in multi-storey construction. The performance of composite structures at elevated temperatures has been studied by researchers across the world [4-7]. The structural behaviour of connections in composite structures in fire is quite different from that of bare-steel connections, due to the existence and continuity of the composite slab. At elevated temperatures, the composite slab acts as insulation to the top part of the connection, reducing its temperature and thus enhancing its performance. The top flange of a composite beam is likely to experience a much lower temperature than the exposed parts, and this temperature difference may even be as high as 40% [8]. Accordingly, the degradation rate of the strength of a composite connection should in general be lower than that of an equivalent bare-steel connection, due to the beneficial effect of this partial temperature reduction. In addition, the composite slab restrains the thermal expansion of the steel beam in the initial stage of a fire, leading to thermal bowing, which also affects the performance of its connections by causing higher early-stage rotations. Leston-Jones [9, 10] conducted three tests on composite flush end-plate connections under constant moment with increasing temperature, to obtain their moment-rotation characteristics across a realistic range of temperatures. AI-Jabri [11] continued Leston-Jones' work by conducting high-temperature tests on two composite flexible end-plate connections of different sizes and developing component-based models of these connections. Liu [12] further developed his three-dimensional finite element model FEAST, which was originally developed to simulate the response of steel structures in fire, to simulate the behaviour of composite connections at elevated temperatures. Li et al. [13] carried out three tests to investigate the fire-resistance of flush end-plate composite joints considering the effect of axial force. After that, they developed a simplified component-based model to calculate the initial stiffness and ultimate moment capacity for flush end-plate composite joints at elevated temperatures [14]. Pucinotti et al. [15] conducted numerical and experimental investigations on welded composite full-strength beam-to-column joints under seismic-induced fires to develop fundamental data for composite beam-to-column joints with concrete-filled tubes.

Current commonly-used connection types lack the axial and rotational ductilities required to accommodate the deformation of a connected beam under fire conditions. In order to improve the performance of connections and enhance the robustness of steel-framed or composite structures in fire, a novel ductile connection has been proposed by the authors [16-19]. A suitable component-based model of the bare-steel ductile connection has been developed and tested by the authors [18] against detailed Abaqus simulations. Therefore, this component-based model has been incorporated into the software Vulcan, and has been used in global frame analyses to test the performance of ductile connections in bare-steel framed structures [19]. Since the behaviour of the ductile connections in bare-steel structures has already been well studied by the authors, it is appropriate now to investigate their performance in composite structures. In non-composite steel frames, the thermal expansion of a complete beam can be absorbed by plastic deformation of the ductile connections, thus greatly reducing the forces imposed on the surrounding structure. However, in composite construction, unless a large number of shear studs are fractured or highly deformed, the deformation of the ductile connections will mainly be caused by rotation at the column face, which will mainly be caused by thermal bowing of the composite beams. Hence the influence of these connections on the overall frame behaviour is less easily predicted.

This paper investigates the application of the ductile connections in composite structures. Equations have been proposed to represent the axial ductility demands of the beam at four key positions; the rebar level, the connection top surface, the connection bottom surface, and the beam bottom flange. In the calculation of ductility demand of the composite beam, the deflection caused by thermal bowing of the composite beam has been included in its total deflection. A reinforcement component, which considers the pull-out of reinforcing bars and the influence of weld points in mesh, has been added to the non-composite ductile connection model to establish a suitable component-based model for the composite ductile connection. This component-based composite ductile connection model has been incorporated into Vulcan, and validated against a detailed Abaqus FE model. Parametric studies using Vulcan have been carried out to study the effect of three parameters on the performance of the ductile connections, including the connection thickness, the inner radius of the semi-cylindrical section and the number of longitudinal reinforcing bars within the effective width of the slab. Since the shear studs are not considered in the component-based composite connection model, an Abaqus model of a plane composite frame has been established to investigate the influence of shear studs on the behaviour of the connection. The method of simulating the composite connection using Abaqus has been validated against experiments carried out by Al-Jabri.

2. The proposed ductile connection

When exposed to fire, connections undergo large axial deformations applied by the connected elements. At the initial stage of a fire, connections are mainly subject to compressive displacement due to the beam's thermal expansion. This eventually changes to tensile displacement when the loss of strength of the connected beam makes it incapable of carrying its load in bending, so that it enters a phase of the tension at very high temperatures. Excessive axial displacement of the connection can lead to fracture, potentially causing the failure of other structural elements, and even the progressive collapse of the entire structure. Therefore, the axial deformation capacity of connections is of great significance in preventing their abrupt failure and improving the inherent robustness of the structure in fire. The design of the proposed connection is based on the concept of ductility demand, which is defined in Section 2.1.

2.1 Ductility demand of composite beam in fire

The deformation of a typical composite beam as its temperature rises is illustrated in Figure 1. The connection needs to be able to accommodate the axial displacement caused by the combined effect of the effective shortening of the beam due to deflection and the rotation of the beam end. In a composite beam, as the slab does not expand with the thermal strain of the steel downstand, the steel's thermal expansion is included in the calculation of the thermal curvature of the composite beam. There are four key positions where the axial displacement of the beam end needs to be taken into consideration; the rebar level, the top surface of the connection, the bottom surface of the connection, and the bottom flange of the beam. The top surface of the connection experiences the maximum displacement away from the column-face, whereas internal contact may occur at the connection's bottom surface. In addition, to avoid contact between the beam bottom flange and column flange, which may lead to the buckling of column web, the axial displacement of the beam bottom flange is also considered when determining the ductility demand. The displacements of these four key positions are represented by Δ_r, Δ_{cts}, Δ_{cbs} and Δ_{bbf} respectively, and can be simply calculated using Equations (1) - (4). The lever arms used are the distances between each key position and the neutral axis of the composite beam. As mentioned previously, the slab restrains the thermal expansion of the composite beam. This leads to thermal bowing, and the deflection due to thermal bowing needs to be included into the total deflection of the composite beam. The total deflection of the composite beam also includes the deflection caused by external load.

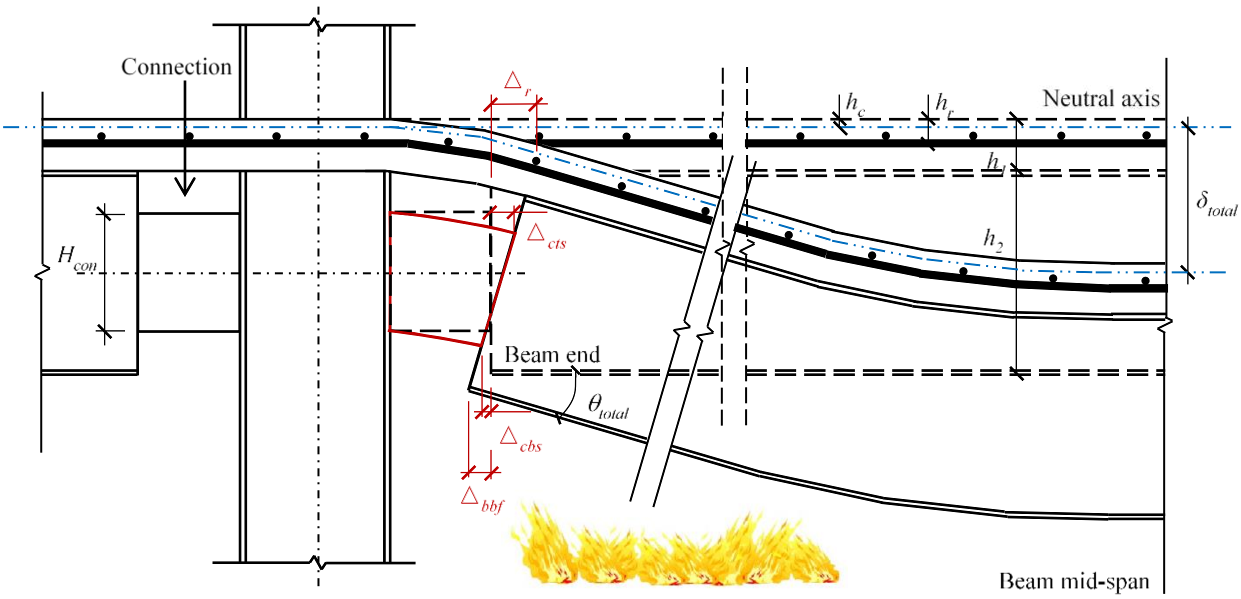

Figure 1. Deformation of composite beam in fire

$$\Delta_r = \frac{4}{3}\delta_{total}{}^2 / l - \tan\left(\theta_{total}\right)\cdot\left(h_r - h_c\right) \tag{1}$$

$$\Delta_{cts} = \frac{4}{3}\delta_{total}{}^2 / l - \tan\left(\theta_{total}\right)\cdot\left(h_1 + \frac{h_2 - H_{con}}{2} - h_c\right) \tag{2}$$

$$\Delta_{cbs} = \frac{4}{3}\delta_{total}{}^2 / l - \tan\left(\theta_{total}\right)\cdot\left(h_1 + \frac{h_2 + H_{con}}{2} - h_c\right) \tag{3}$$

$$\Delta_{bbf} = \frac{4}{3}\delta_{total}{}^2 / l - \tan\left(\theta_{total}\right)\cdot\left(h_1 + h_2 - h_c\right) \tag{4}$$

To calculate the thermal bowing deflection of the composite beam, several assumptions are made here:

1) the slab is assumed to remain at ambient temperature;

2) the temperature distribution within the beam section is uniform;

3) full shear connection between the slab and steel beam is assumed.

As shown in Figure 2 (a), the mechanical strain is obtained by subtracting the thermal strain from the total strain, and is then used to establish mechanical equilibrium.

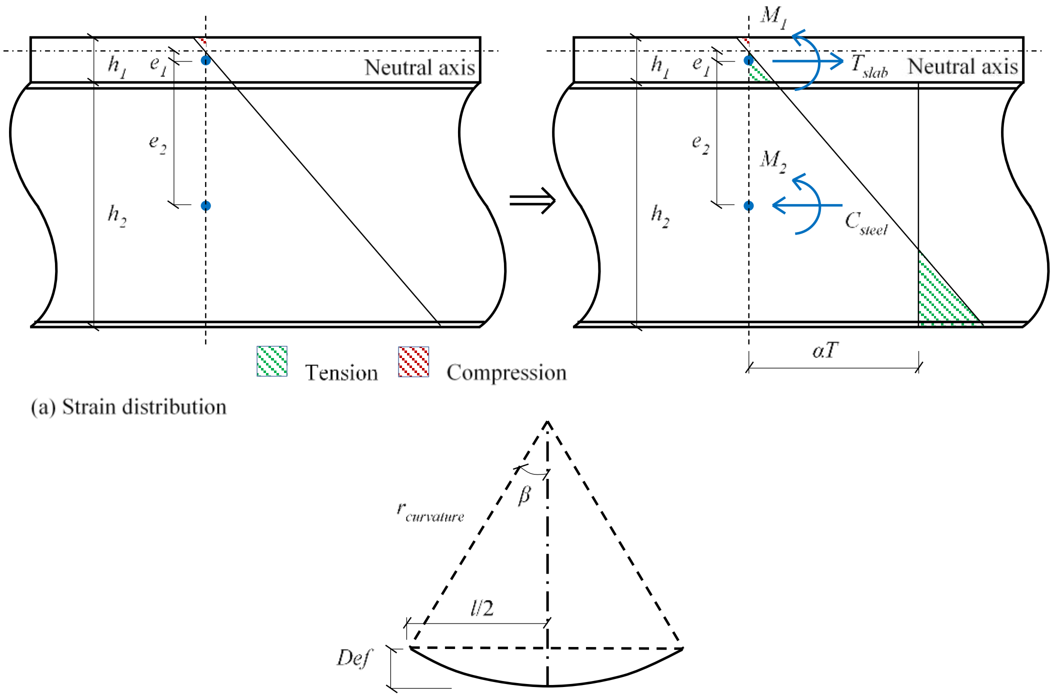

(a) Strain distribution

(b) Calculation of deflection

Figure 2. Calculation of the thermal bowing deflection of composite beam

Due to the assumption of full shear connection, the curvature of the slab is equal to that of the beam (Equation (5)).

$$\frac{M_1}{E_1 I_1} = y'' \qquad \frac{M_2}{E_2 I_2} = y'' \tag{5}$$

The tensile force acting at the centroid of the slab T_{slab}, and the compressive force acting at the centroid of the steel section C_{steel} can be obtained using Equation (6).

$$T_{slab} = E_1 A_1 y'' e_1 \qquad C_{steel} = E_2 A_2 (\alpha T - y'' e_2) \tag{6}$$

According to the horizontal force equilibrium, the curvature can be expressed by a formula containing the two distances e_1 and e_2 from the neutral axis to the centroids of the slab and steel section respectively (Equation (7)).

$$T_{slab} = C_{steel} \Rightarrow E_1 A_1 y'' e_1 = E_2 A_2 (\alpha T - y'' e_2) \Rightarrow y'' = \frac{E_2 A_2 \alpha T}{E_1 A_1 e_1 + E_2 A_2 e_2} \tag{7}$$

Moment equilibrium is then used to obtain the values of e_1 and e_2, as shown in Equation (8).

$$T_{slab}\frac{h_1+h_2}{2}=M_1+M_2 \Rightarrow e_1=\frac{2(E_1I_1+E_2I_2)}{E_1A_1(h_1+h_2)} \quad e_2=e_1+\frac{h_1+h_2}{2} \tag{8}$$

Once the curvature is determined using Equation (7), the deflection due to thermal bowing is calculated using Equation (9). The variables in Equation (9) are illustrated in Figure 2 (b).

$$\beta=\sin^{-1}\left(\frac{l/2}{r_{curvature}}\right) \qquad Def=r_{curvature}(1-\cos\beta) \tag{9}$$

An example composite beam of 10 m span, subject to a uniform load intensity of 20 kN/m^2 applied on top of the slab is used to demonstrate the determination of ductility demand. The steel downstand of the composite beam is designed as a UKB 533×210×109. The depth and width of the slab are 130 mm and 2600 mm, respectively. It should be noted that the width used here is the effective width of the concrete flange of the composite beam, which is $b_{eff}=l/4+b_0$, where b_0 represents the width of the steel flange occupied by shear studs. After the position of the neutral axis of the composite beam is obtained, the thermal bowing deflection and the displacements of the four key positions are calculated using Equations (1)-(9), and are shown in Figure 3. This figure shows that the connection should have an axial deformation capacity of at least 28.1 mm in "closing" and 10.7 mm in "opening", in order to meet the ductility demand of the composite beam in fire, if the composite beam is designed to survive to 800 °C. The elastic modulus of steel decreases with the increase of temperature. When the temperature reaches 600°C, the elastic modulus of steel decreases considerably, to the same order of magnitude as that of concrete, which leads to the rapid change of thermal bowing deflection slope, as shown in Figure 3 (a).

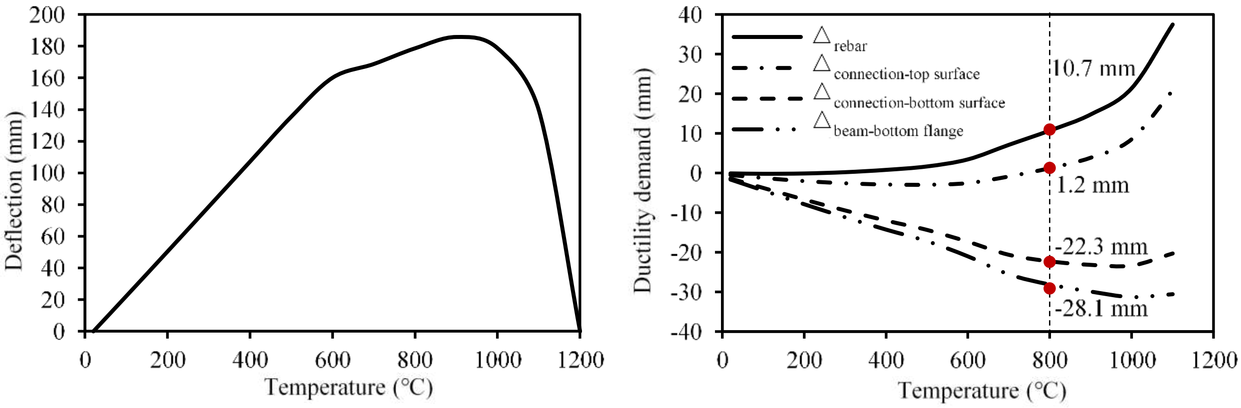

(a) Thermal bowing deflection (b) Ductility demand

Figure 3. Determination of ductility demand of the example composite beam

2.2 Design of the ductile connection

To meet the ductility demand of the beam in fire, a novel ductile connection has been proposed by the authors [16-19]. This novel connection consists of two identical opposed parts. Each part includes a fin-plate bolted to the beam web, a face-plate bolted to the column flange, and a semi-cylindrical section between the fin-plate and the face-plate to provide additional ductility by allowing the fin-plate to move towards and away from the face-plate, as shown in Figure 4. The most critical parameter of the ductile connection in terms of the ductility demand in fire (Equations (1)-(4)) is the diameter of the semi-cylindrical section. All other parameters, such as the thickness and depth of the plate and the number of bolt rows, can be determined in accordance with EC3 [3].

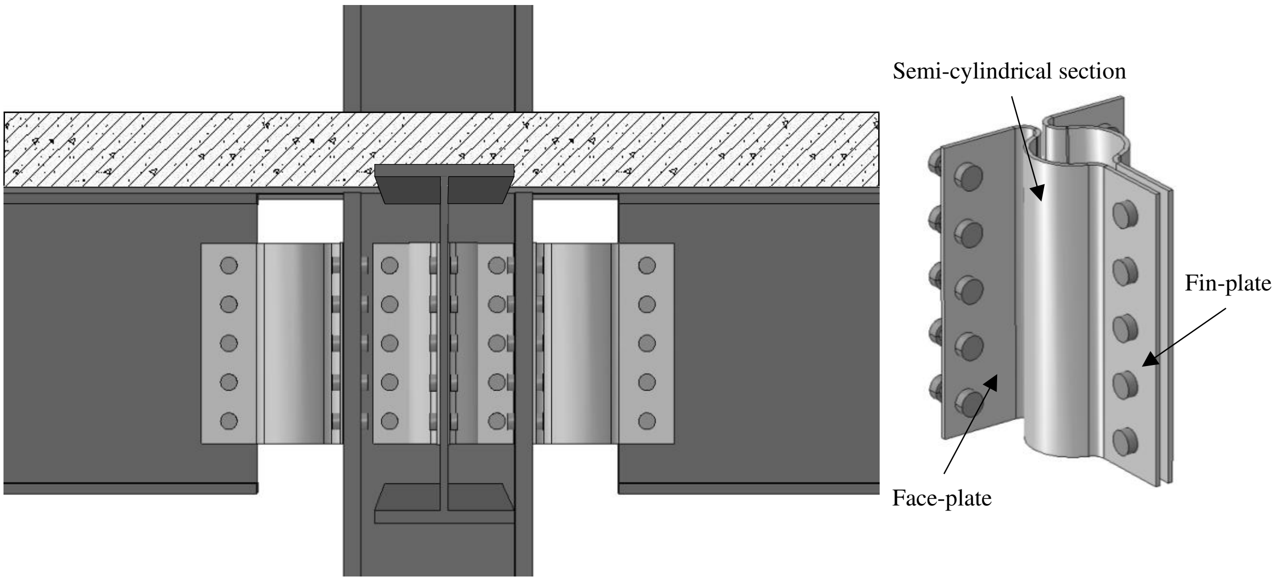

Figure 4. The schematic of the ductile connection

3. Component-based model of the composite ductile connection

Component-based modelling of bare-steel connections has been well studied in recent years. However, few studies have been conducted on the component-based modelling of complete composite connections. Madas [20] proposed a component-based model of composite end-plate connections for use in the analysis of composite frames under dynamic loading at ambient temperature. In the Madas model, the concrete slab is divided into a finite number of layers and each layer considered is subject to a uniform strain between studs and across the slab's effective width. Al-Jabri [11] developed a high-temperature composite end-plate connection model by adding two additional components, representing the reinforcement and shear studs, to his steel end-plate component-based connection model. Rassati et al. [21] developed an ambient-temperature component modelling approach for the simulation of composite connections, which is capable of accounting for the influence of partial interaction between the slab and beam, and the cracking and crushing of the slab. Li et al. [14] developed a component model, which includes bolts in tension, reinforcement in tension, end-plate in bending, column flange in bending and column web in compression, to predict the initial stiffness and the ultimate moment capacity of composite connections in fire. However, the component-based models reviewed above are mainly for composite end-plate connections, and cannot be directly applied to the composite ductile connection. In addition, the full load-deformation characteristics of the connection, including the axial deformation of each spring row in the process of connection deformation, are needed to investigate the performance of the ductile connection as part of a composite structure; these are not available in existing models. It was, therefore, decided to develop a component-based model of the composite ductile connection in this research.

A component-based model of the non-composite ductile connection has already been developed by the authors [18] and has been implemented into the Vulcan software for global frame analysis [19]. Vulcan is a finite element software developed by the Structural Fire Engineering Research Group at the University of Sheffield. It can be used to simulate the behaviours of 2-D or 3-D bare-steel and composite structures at elevated temperatures, considering both geometrical and material non-linearities. The 2-noded spring element in Vulcan can model ideally rigid or pinned connections, as well as the traditional connection types (e.g. end-plate connections) using a component-based method. Using the same method as the bare-steel ductile connection, the composite ductile connection will be implemented into Vulcan as a 2-noded spring element. Since the connections are within the hogging bending moment zone, and the tensile strength of concrete is negligible, the concrete in tension is ignored. In the following section, a reinforcement component is added to the non-composite ductile connection model to establish a suitable model of the ductile connection in a composite structure. This component-based composite ductile connection model has also been incorporated into Vulcan, and several case studies are carried out to test its performance.

3.1 Reinforcement component

Depending on its effective depth within the slab, the reinforcement above the connection may be subject either to tensile or compressive strain due to the combination of hogging moment and thermally-induced rotation. In the case where the reinforcement strain becomes tensile, as the tensile strength of the concrete is very low, cracks usually occur, leading to reinforcement pull-out within these cracks. The part of the rebar within the crack width is under uniform stress, which is equal to its ultimate strength. However, the part of the rebar within the embedded length is subject to stresses lower than those within the crack width, due to the surface bond stress. The further away from the crack-face, the smaller the stress is. Sezen and Setzler [22] considered the pull-out of the rebar at concrete cracks when modelling the lateral deformation of a column caused by rebar slip in the anchorage zone. Their simple model of rebar slip, shown in Figure 5 (a), was verified against 12 tests conducted by Sezen [23] and by Lynn et al. [24].

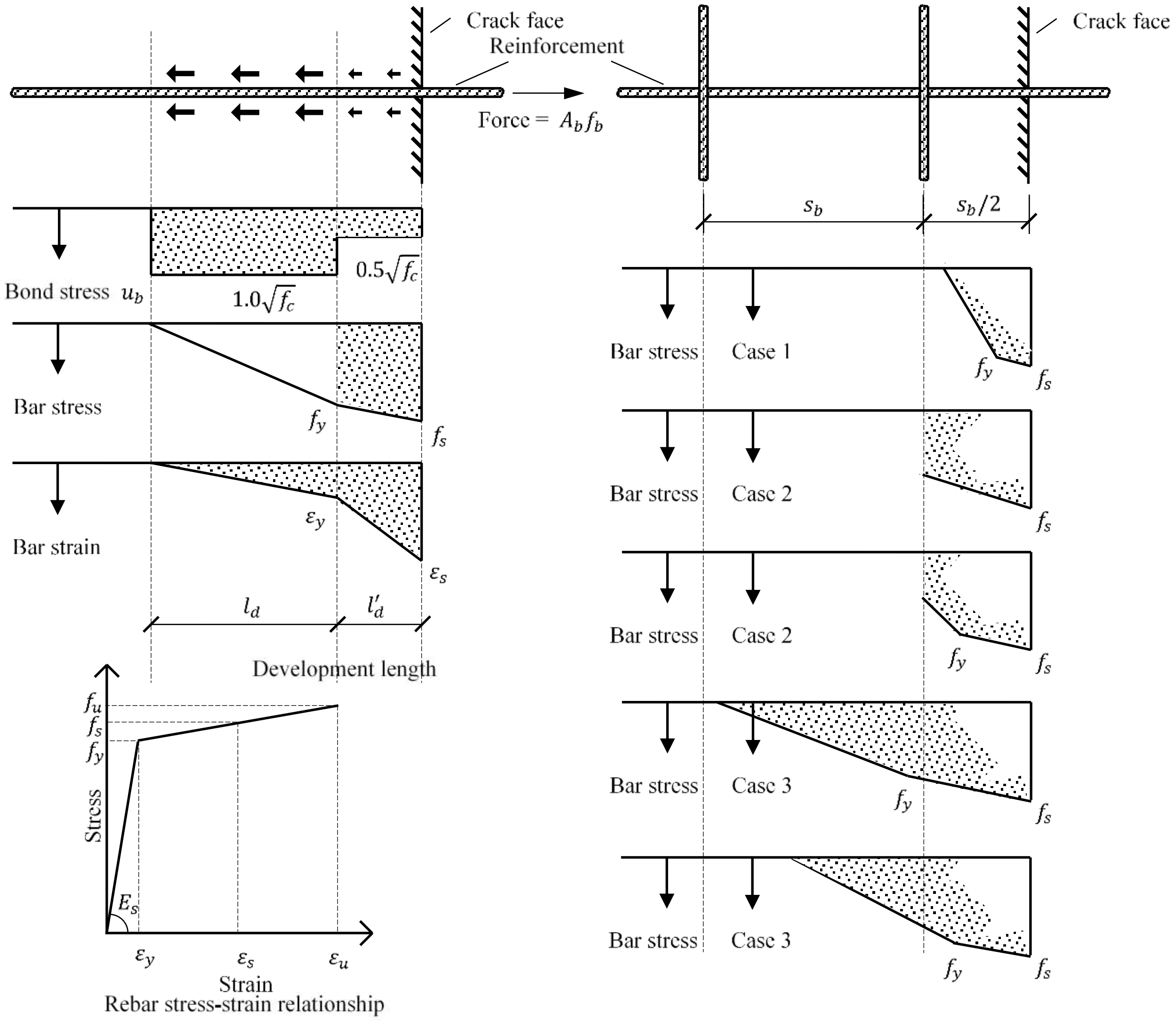

(a) Rebar slip model[22]

(b) Different cases considering the anchorage of the welds

Figure 5. Model of the rebar component

In this model, a bilinear stress-strain relationship is assumed for the rebar, with a shallow gradient between the yield and ultimate stress points. The bond stress within the embedded length is assumed to be locally constant, at either u_b and u'_b. When the rebar strain is lower than the yield strain, the bond stress is $u_b = 1.0\sqrt{f_c}$, but when the rebar strain is above yield, the bond stress is $u'_b = 0.5\sqrt{f_c}$. This assumption is reasonable because only high rebar strain (above yield) and the resulting high slip at the rebar perimeter can cause real damage to the adjacent concrete. The slip of the rebar can be calculated using Equations (10) and (11). In the extreme case of rebar fracture within the crack, $f_s = f_u$ and $\varepsilon_s = \varepsilon_u$. In the context of Figure 5,

$$l_d = f_y d_b / 4u_b \qquad l'_d = (f_y - f_s) d_b / 4u'_b \tag{10}$$

The total slip of the rebar from the crack-face, assuming that it is anchored in the concrete either side of the crack is

$$slip = \varepsilon_y l_d / 2 + (\varepsilon_s + \varepsilon_y) l'_d / 2 \tag{11}$$

Burgess [25] further considered the contribution of the weld points on the transverse reinforcing bars in the mesh when calculating the crack width at which rebar fractures using the simple slip model presented above. In fact, the weld points on the transverse bars at regular spacing s_b can provide physical anchorages to the longitudinal bars. The strength of each weld should be at least 25% of the bar strength in accordance with Eurocode 2 [26]. If the rebar stress at a weld point exceeds the strength of the weld, then the weld will fracture. The distance from the crack-face to the next weld point is then used as the development length. In this case, the pull-out of the rebar will increase suddenly when weld fracture occurs. Considering different combinations of development length, rebar stress and weld strength, three typical cases are shown in Figure 5 (b). The first weld is positioned at a distance of $s_b / 2$ from the crack face, and the subsequent welds are at a regular spacing s_b. In Case 1, the development length of the rebar does not go beyond the first weld; this is likely to occur to deformed bars with very high bond stress. If the development length reaches the first weld-point, there are two possible scenarios, according to the relationship between the rebar stress and the weld strength.

1) <u>Case 2:</u> If the rebar force is less than or equal to the weld strength, the first weld does not fracture, but becomes a positive anchorage point. The development length and crack width are both reduced compared to when weld points are neglected;
2) <u>Case 3:</u> If the rebar force exceeds the weld strength, the first weld fractures and the remaining anchoring force is borne by the bond stress developed beyond the broken weld. For bars with low bond stress, such

as plain circular bars, there may be more welds broken before sufficient anchorage is accumulated.

According to Burgess's study [25], for plain rebars the bond stresses are reduced to $u_b' = 0.15\sqrt{f_c}$ and $u_b = 0.3\sqrt{f_c}$. For deformed bars, the two values ($u_b' = 0.5\sqrt{f_c}$ and $u_b = 1.0\sqrt{f_c}$) mentioned earlier remain valid. The weld strength is assumed to be 25% of the rebar strength according to Eurocode 2 [26].

The force-slip curve of a bar is generated by using the rebar slip model considering the weld anchorage described above. If the concrete crack occurs in the middle of the slab and there is enough length on both sides of the crack to develop the anchorage, the crack-width should be twice the slip from a single crack face. The tensile force of the rebar is obtained by multiplying the rebar stress by its cross-sectional area. Taking deformed and smooth A252 meshes at 200 mm × 200 mm spacing as two examples, the properties of these two meshes and their weld fracture predictions are listed in Table 1.

The calculated force-slip curves are shown in Figure 6 (a). This figure shows that only the first weld of the deformed A252 breaks, whereas three successive welds break for the smooth A252 bar. The location of the concrete crack must be determined when the rebar component is incorporated into the component-based model of the connection. Based on the results of the tests conducted by Al-Jabri [11], it is assumed that the crack occurs on the outer surface of the column flange, as shown in Figure 6 (b).

Table 1. Properties of deformed and smooth A252 meshes and the weld fracture predictions

Rebar type	Diameter (mm)	Ductility class	Strengths (MPa)		Ultimate strain	Weld fractures		
			f_y	f_u	ε_u	1st	2nd	3rd
Deformed A252	8	C	435	500	0.075	Y	N	N
Smooth A252	8	C	435	500	0.12	Y	Y	Y

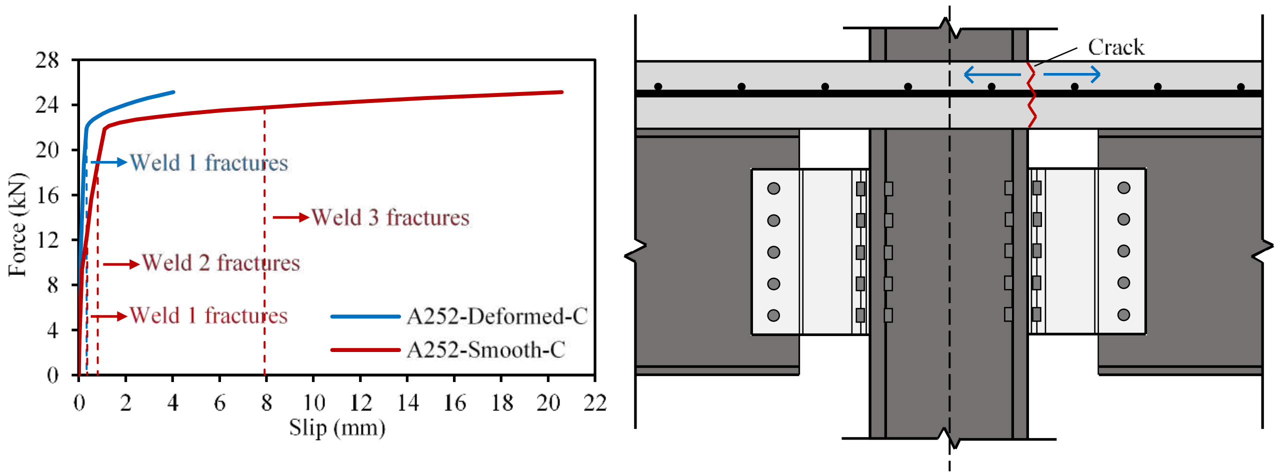

(a) Force-slip curves of two different types of meshes

(b) Development length of rebar component

Figure 6. Rebar component

The development length on the right side of the crack is assumed to be limited by the first three weld points, since previous research indicates that the rebar development length usually does not exceed the third weld point [25]. The development length on the left side of the crack is assumed to be limited by the first weld point and the centre line of the column section, depending on whether the first weld point fractures. The slip on the left and right sides of the crack should be calculated separately. The sum of the slips on both sides is the crack-width, or the total displacement of the rebar component.

3.2 Incorporation of the component-based model into Vulcan

The rebar component described above has been added to the component-based model of the bare-steel connection [18, 19] to form the component-based model of the composite ductile connection. As shown in Figure 7 (a), the proposed component-based model includes components representing the face-plate and cylindrical section, the column web in compression, bolt pull-out, rebar, fin-plate in bearing, beam web in bearing and bolt in shear. The gap between the compression spring row and the column face is designed to represent the maximum compressive displacement before internal contact occurs. The component-based model is then converted into a connection element, following the principles of the finite element method. The method is introduced in detail in a previous paper [19], and so is not repeated here. The 2-D composite frame model shown in Figure 7 (b) is used to test the performance of the composite connection element. The height of the upper and lower columns is 3 m, and the beam span is 10 m. The rebar is assumed to be anchored to the centre line of the column section for both the inner and outer column cases. For an inner column, the inherent symmetry of deflection about the column line makes this assumption generally valid. For the outer column case, the rebar is assumed to be anchored, generally by a hook, to the column, which would be normal good design practice. In order to reduce the size of the model to save computation cost, only half of the frame is modelled, and symmetric boundary conditions are applied at the mid-span of the beam and slab. The bottom of the column is fully restrained, and the top can only move vertically. It is further assumed that fire only occurs in the lower storey. Lawson [27, 28] assumed that the temperature of the connection was about 70% of that of the beam bottom flange at the beam mid-span. This assumption applies to bare-steel structures. Since the concrete slab can act as an insulation to the connection, it was decided to further reduce the connection temperature to half of the beam temperature in the 2-D composite sub-frame model. Columns in steel-framed structures are invariably protected, and so the temperature of the lower column is set to be equal to the connection temperature, assuming that they are protected to the same level. The slab and the upper column are assumed to remain at ambient temperature. Full shear connection is assumed between the slab and beam, and this is modelled by shared nodes between the slab and beam elements. In order to verify the developed connection element, an Abaqus 2-D composite frame model is also established. The Abaqus modelling approach is described in Section 4, including material characteristics, contact settings, etc. The only difference is that the shear studs in the Abaqus model are not modelled in detail in this section. Full shear connection is achieved by fully tying the bottom of the slab and the top flange of the steel beam. The deformations of the ductile connection at different temperatures obtained from the Abaqus model is shown in Figure 8 for a perimeter column connection. As can be seen from this figure, the proposed ductile connection exhibits satisfactory deformability.

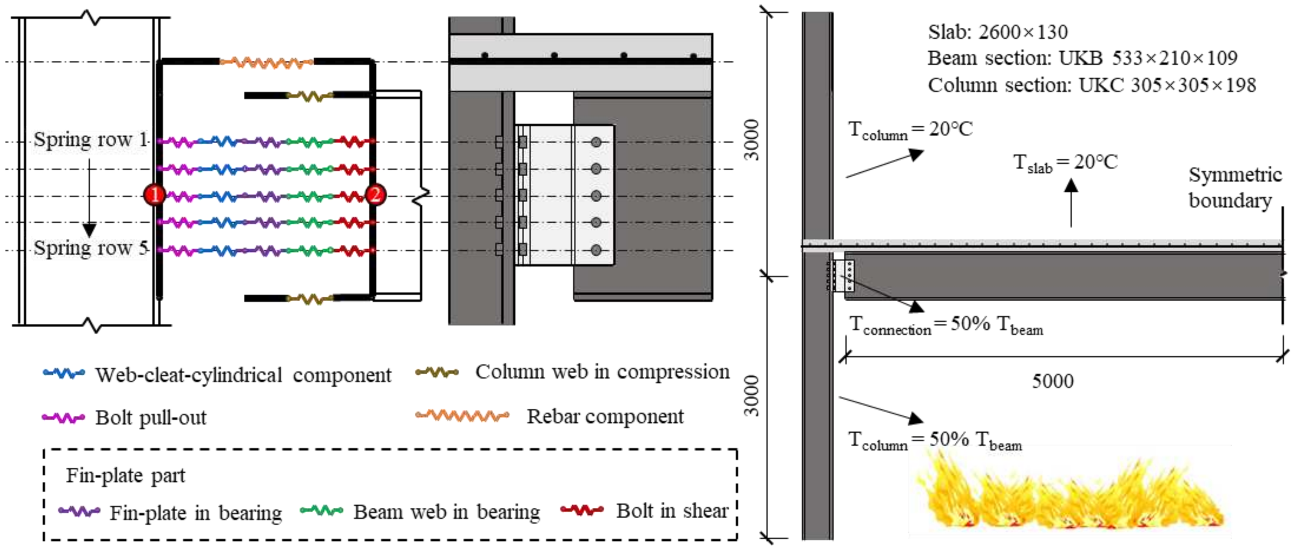

(a) The proposed component-based model (b) The 2-D composite frame model

Figure 7. The component-based model and the 2-D composite frame model

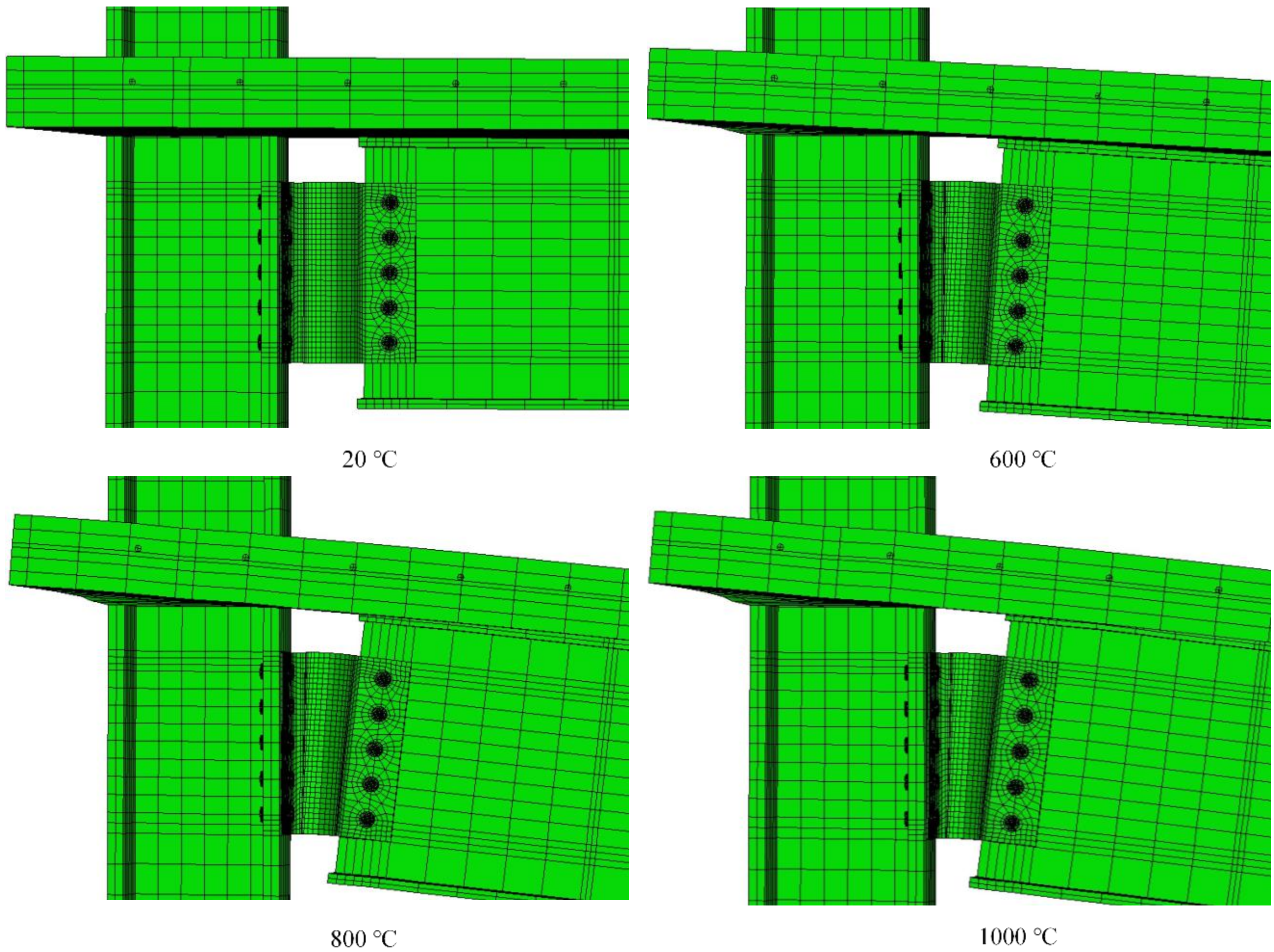

Figure 8. Deformation of the ductile connection at different temperatures; connection to a perimeter column.

The results of the Abaqus and Vulcan models are compared in Figure 9. Looking at the mid-span deflections and end rotations shown in Figure 9 (a) and (b), the Abaqus model appears to be stiffer than the Vulcan model at temperatures above 200 °C. These differences can be explained by two different aspects of the respective models:

1) In its plastic phase, the push-pull analytical model of the semi-cylindrical section used in the component-based model of the ductile connection is softer than the detailed Abaqus connection model [16], as shown in Figure 9 (d);
2) The concrete cracking and the pull-out of reinforcing bars are only introduced in the Vulcan connection element; they are not considered in the Abaqus model, making the composite slab of the Abaqus model apparently stronger than that of the Vulcan model.

The differences between the Abaqus and Vulcan models occur above 200 °C, since all the spring rows of the Vulcan connection element are within their linear-elastic phase below 200 °C, and the difference between the push-pull analytical model used in Vulcan and the detailed Abaqus model in the linear-elastic range is small (Figure 9 (d)). The comparison of the connection axial forces obtained from the Vulcan and Abaqus models is shown in Figure 9 (c), which shows that above 200 °C the connection axial force of the Abaqus model is larger than that of the Vulcan model. This is also due to the fact that the Abaqus detailed connection model is more rigid than the push-pull analytical model in the plastic stage. At around 690 °C, the compressive axial force of the connection in the Vulcan model decreases rapidly and changes temporarily into tension at about 800 °C. Above this temperature, the connection axial force becomes compressive again. During heating, the behaviour of the connection is affected by the combined effects of thermal expansion and material degradation. In the beam temperature range 700 °C - 800 °C, the change of steel crystal structure causes a pause in the beam's thermal expansion, which resumes when the transition is complete. This can be seen (Figure 9 (b)) to cause a temporary change of direction in the connection rotation. This causes the connection spring rows to reverse direction, causing their forces to change rapidly into tension because of the rather stiff nature of the elastic unloading curves [18]. When the thermal expansion recommences, the connection force again rapidly changes to compression, as shown in Figure 9 (c). Figure 10 (a) and (b) show the temperature-force and temperature-displacement curves of each spring (component) row in the Vulcan model, indicating that the decrease in connection rotation leads to unloading of all the spring rows. Among all the five spring rows, the reduction in the compressive displacement of the bottom spring row (Row 5) is the largest, whereas the displacement reduction of the top spring row (Row 1) is the smallest. Therefore, Row 5 enters the so-called pulling-back stage [18], and its force temporarily changes into tension, whereas Row 1 is within the unloading stage before the compressive displacement increases again, and its force remains as compressive.

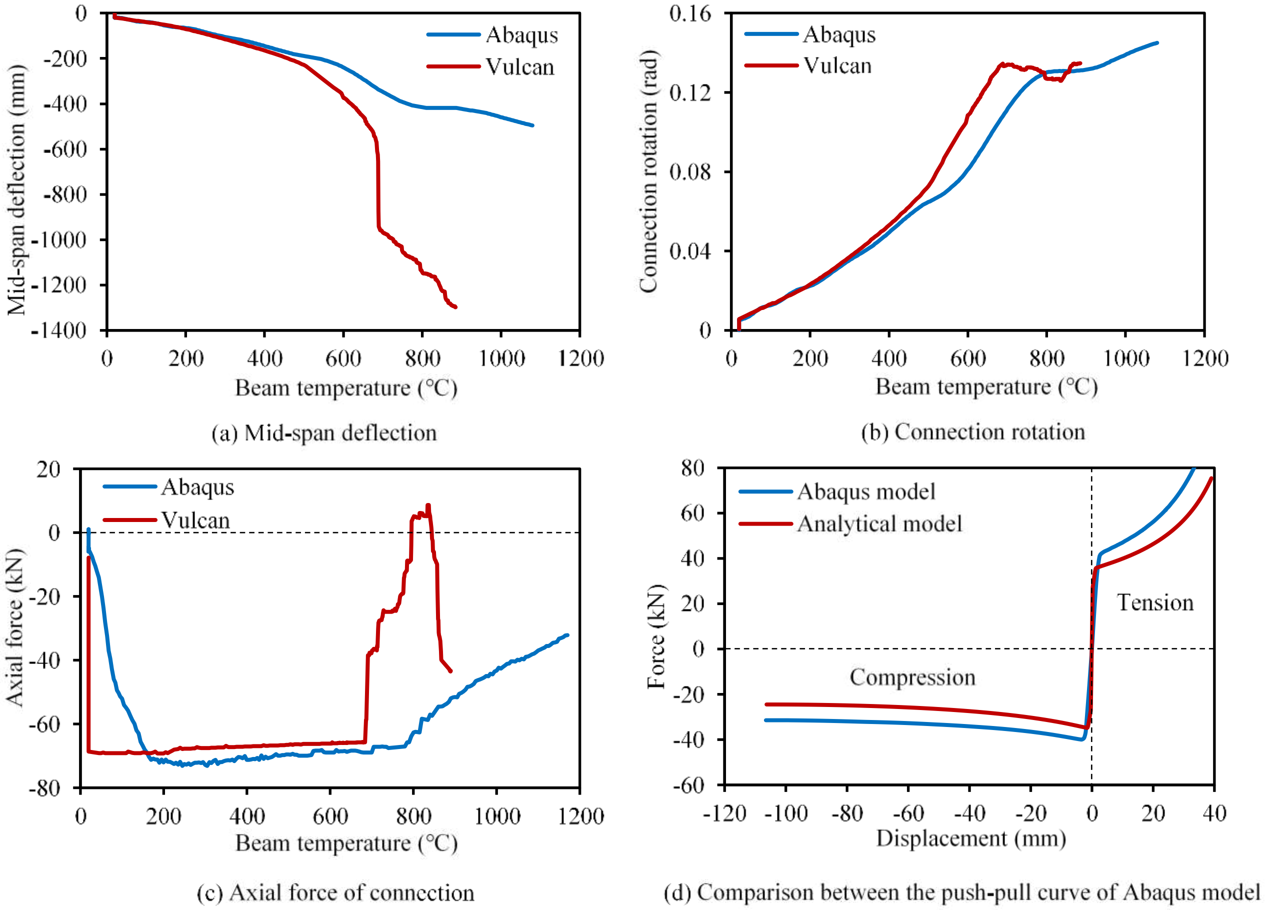

(a) Mid-span deflection

(b) Connection rotation

(c) Axial force of connection

(d) Comparison between the push-pull curve of Abaqus model and that of analytical model

Figure 9. Comparison between Vulcan and Abaqus

Figure 10 (c) and (d) show the temperature-force and temperature-displacement curves of the rebar component of the Vulcan model, which works only in tension. It is temporarily active at ambient temperature due to the hogging moment applied to the connection; it then remains inactive until about 600 °C, since the beam’s thermal expansion compensates for the tensile displacement of the rebar component. After the activation of the rebar component, the discrepancy between results from the Vulcan and Abaqus models begins to increase, as shown in Figure 9 (a) and (c). At 689 ℃, the force in the rebar component increases almost vertically; this is caused by a sudden increase of beam deflection (shown in Figure 9 (a)), as all the spring rows enter the unloading stage, which is manifested by the sudden decrease of the compressive forces of all the spring rows, as shown in Figure 10 (a). Most Vulcan results show a slight oscillatory pattern, which is caused by the large unloading stiffness of the connection element. It is assumed that the unloading stiffness of the spring row in the connection element is the same as the initial elastic loading stiffness, and the initial elastic loading stiffness of the ductile connection is very large [18]. This leads to a sudden change of the spring force when unloading occurs, which is manifested by the slight oscillatory pattern of the Vulcan result curves. In addition to this, the concrete model used in the slab elements models cracking at different levels within the elements. This causes the tensile stresses at various locations to vanish abruptly as the loading or heating proceeds. In general, the performance of the Vulcan connection element is satisfactory compared with the detailed model in Abaqus, indicating that the Vulcan composite connection element which has been developed can be used to investigate the effect of utilising the ductile connection within a composite structure in fire conditions.

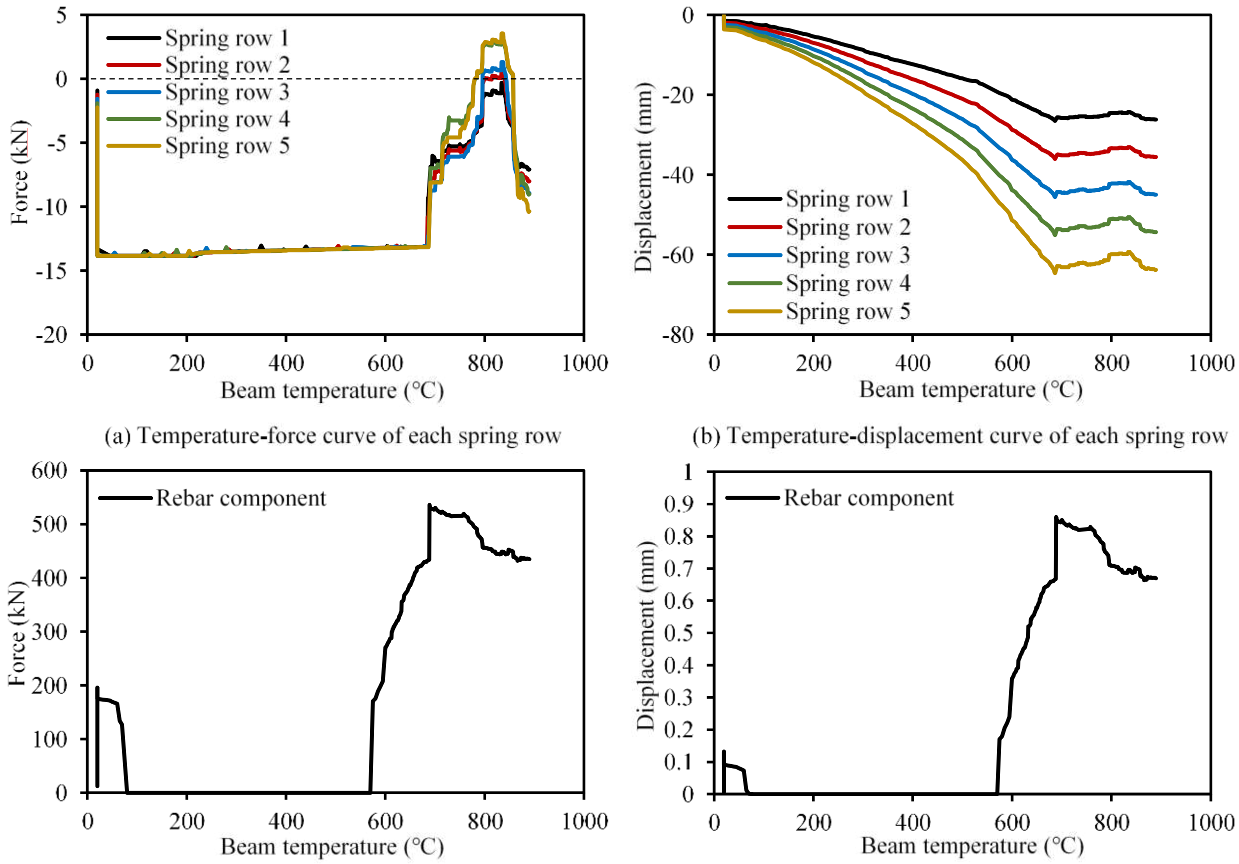

(a) Temperature-force curve of each spring row

(b) Temperature-displacement curve of each spring row

(c) Temperature-force curve of rebar component

(d) Temperature-displacement curve of rebar component

Figure 10. Temperature-force and temperature-displacement curves of each spring row and rebar component

3.3 Parametric studies using Vulcan

In this section, the 2-D composite frame model shown in Figure 7 (b) is used for a series of parametric studies. The effects of three parameters (the connection thickness, the inner radius of the semi-cylindrical section and the number of longitudinal bars within the effective width of the slab) are studied. As shown in Figure 11, an increase in connection thickness leads to a decrease in connection ductility. Frames experience lower mid-span beam deflection, smaller connection rotation, larger connection axial force, larger rebar component force, and smaller axial displacement at the beam end, as their plate thickness increases. As mentioned previously, the inner radius of the semi-cylindrical section is a key parameter, determining the connection's axial deformation capacity, and should be determined on the basis of the ductility demands obtained using Equations (1) - (4).

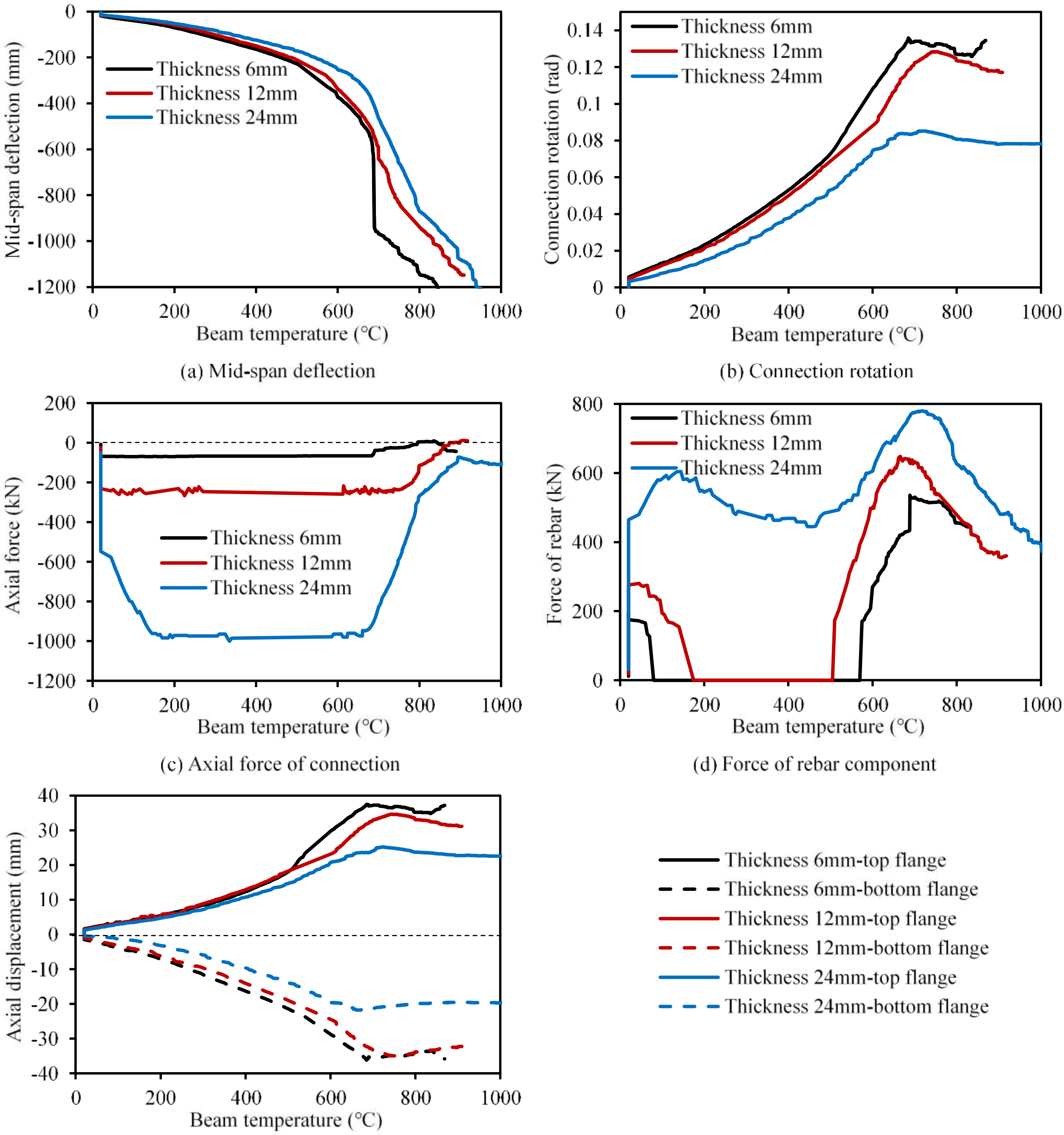

(a) Mid-span deflection

(b) Connection rotation

(c) Axial force of connection

(d) Force of rebar component

(e) Axial displacement at beam end

Figure 11. Different connection thickness

The effect of the semi-cylindrical section's inner radius on the connection's behaviour is shown in Figure 12. This figure shows that connections with larger inner radii have higher axial ductility, which can significantly reduce the forces in the connection and reinforcing bars, compared with connections of smaller inner radii. However, the influence of the cylindrical section radius on the mid-span beam deflection, connection rotation and beam end axial displacement are not obvious below about 500 °C. Above 500 °C, the mid-span beam deflection and connection rotation of the composite frame models with larger cylindrical section radius are smaller than those of the same frame with smaller radii. Although increasing the cylindrical section radius can effectively improve the axial deformation capacity of the ductile connection, it should be noted that an excessive increase in this radius may hinder the installation of bolts in the end-plate part of the connection, and may lead to hard contact between the semi-cylindrical section and the end-plate. Therefore, the limitation on the dimensions of the various parts of the ductile connection does not generally depend on the analytical aspects of its behaviour, but on the constraints of practical construction.

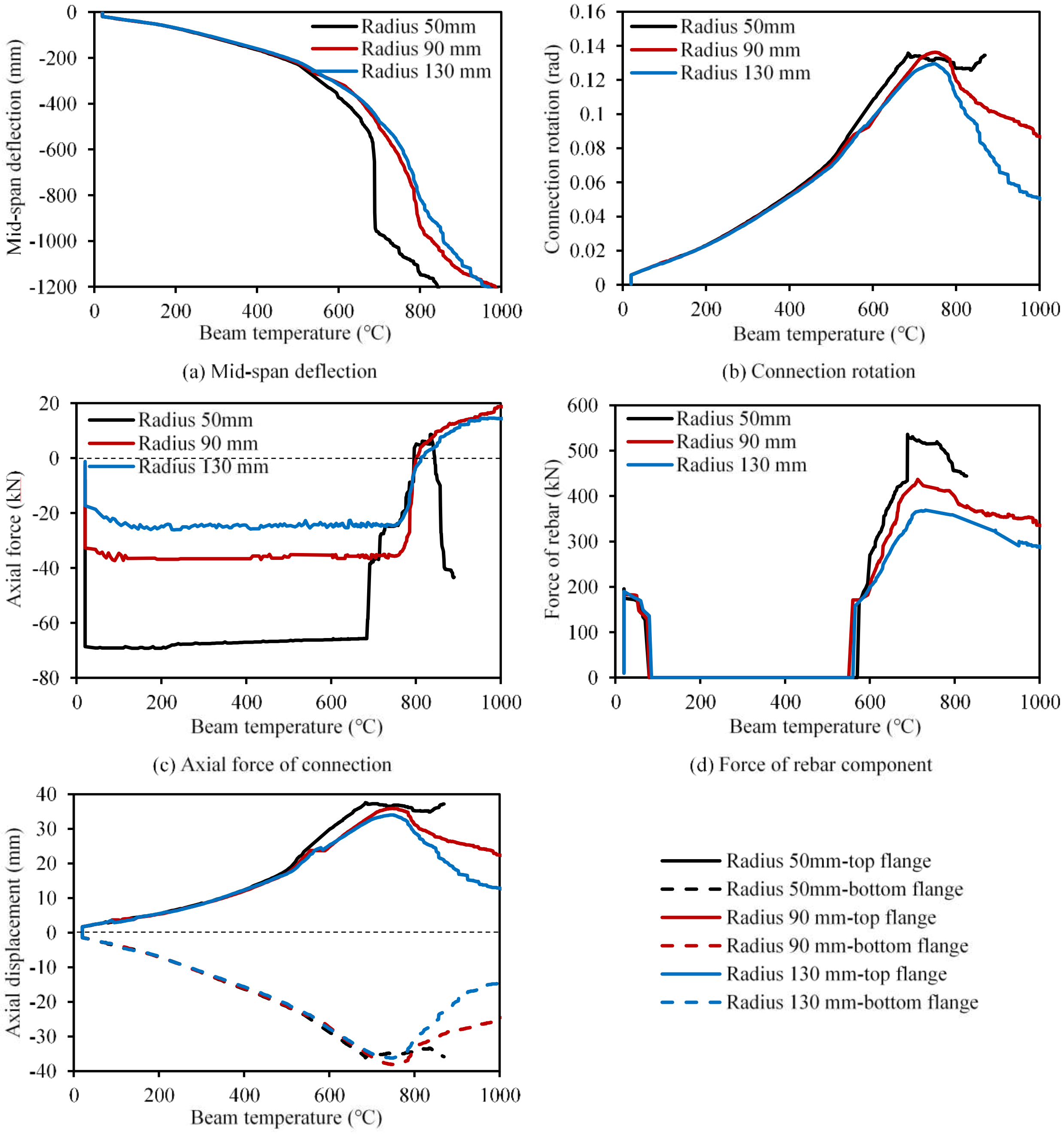

(a) Mid-span deflection

(b) Connection rotation

(c) Axial force of connection

(d) Force of rebar component

(c) Axial displacement at beam end

Figure 12. Different inner diameter of the semi-cylindrical section

The difference between the component-based model of the bare-steel ductile connection and that of the composite version is the introduction of the rebar component. Therefore, the effect of the number of longitudinal bars on the behaviour of the composite connection is also worth attention. In general, composite ductile connections with fewer longitudinal bars are prone to premature failure. It can be seen from Figure 13 (a) and (b) that the mid-span beam deflection and connection rotation of the composite frame model with 7 bars increase rapidly at 688 ℃. This is caused by the failure of the rebar component (Figure 13 (d)). The connection axial force of this model changes suddenly from compression to tension at 688 ℃, when the bars fail, and then carries on increasing in tension from this point (Figure 13 (c)). At the same time, the axial displacement of the beam bottom flange at beam end changes from compressive to tensile, which is a first indication of run-away failure of this model.

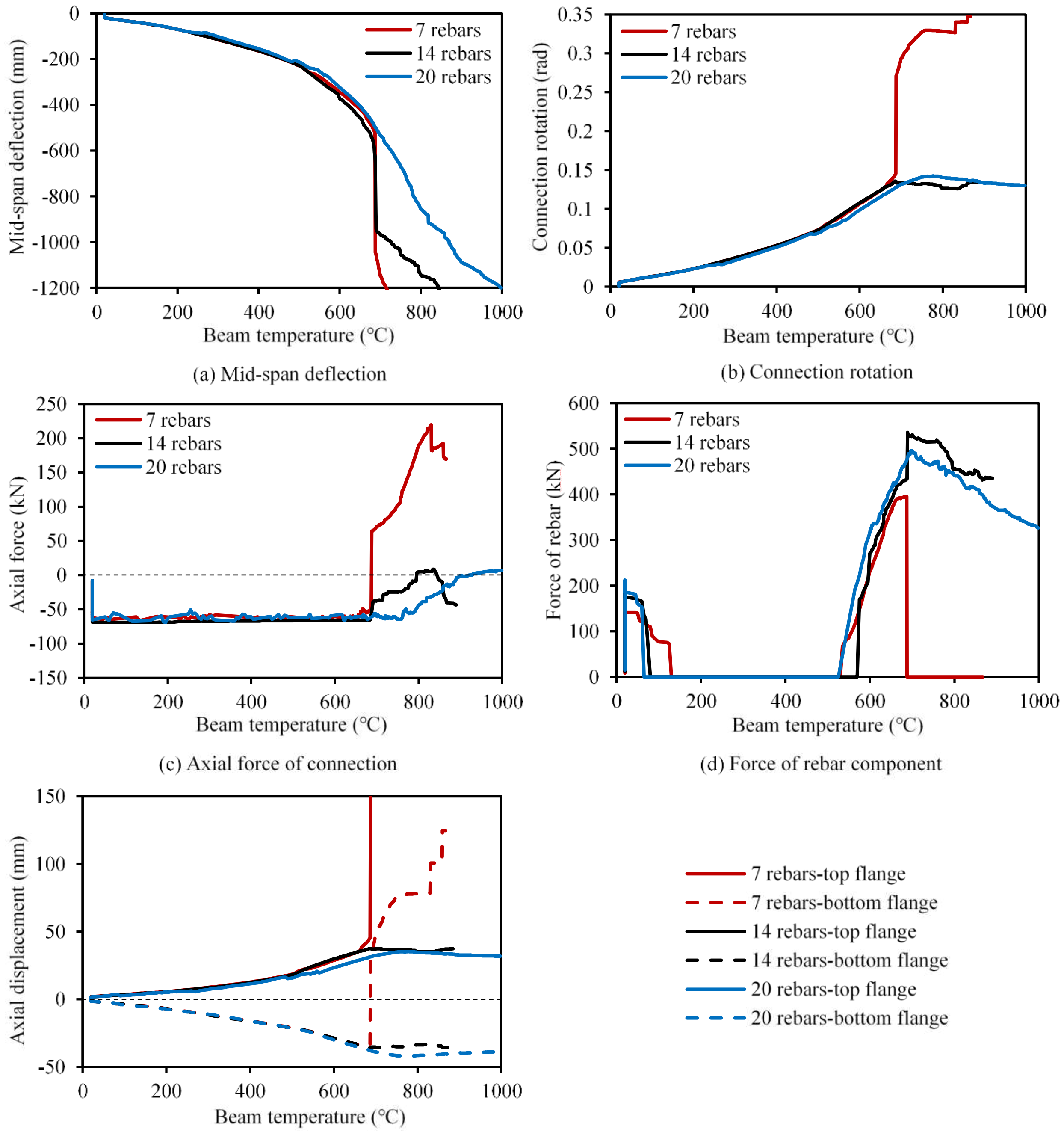

(e) Axial displacement at beam end

Figure 13. Different number of longitudinal rebars

Figure 14 shows the temperature-force and temperature-displacement curves of each spring row of this model. Row 1 fails at 831 °C, at which point the forces in the remaining spring rows increase suddenly. Among these, the force increase in Row 2 is the largest, and this spring row fails at a slightly higher temperature (859.5 °C). The failure of Rows 1 and 2 results in an increase of connection rotation and the axial displacement at the beam end in a stepped manner, as well as a stepped decrease in connection axial force, as shown in Figure 13. Although increasing the number of longitudinal bars can effectively delay the failure of the composite ductile connection, the additional cost of doing so should also be considered. In addition, the spacing of rebars should not be less than the minimum spacing specified in the Eurocode. The minimum spacing of reinforcing bars should be greater than the reinforcing bar size, the maximum aggregate size + 5mm or 20mm [29]. In the immediate vicinity of the connection the spacing has to be sufficient to bypass the column with an adequate clearance.

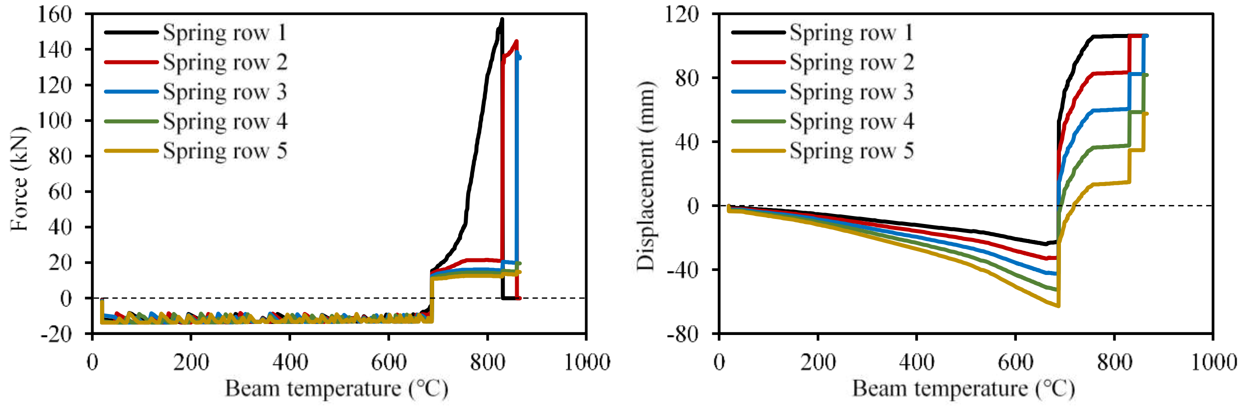

(a) Temperature-force curve of each spring row (b) Temperature-displacement curve of each spring row

Figure 14. Result curves of each spring row in the model with 7 rebars

4. Abaqus sub-frame model

The function of shear studs is to connect the slab and steel beam, transmitting the horizontal shear force between the two. The moment capacity of the composite beam can be reduced if partial-strength shear connection is applied. Therefore, shear studs are very important components in composite structures. It is therefore useful to investigate the influence of shear studs on the performance of the composite ductile connection. However, the shear studs are not included in the Vulcan composite connection element, and so it was decided to establish a composite frame model (Figure 7 (b)) in Abaqus to study the influence of shear studs. The behaviour of the steel decking on which the concrete is cast cannot be guaranteed in a fire. The thin steel deck heat much more quickly than the concrete, and usually separates from it under the influence of its own local thermal expansion. The steel deck is of little importance at high temperatures, and is therefore neglected to simplify the Abaqus model, and to save computational cost.

4.1 Concrete material model

The nonlinear behaviour of uniaxially compressed concrete at different temperatures is represented by a series of stress-strain curves as shown in Figure 15.

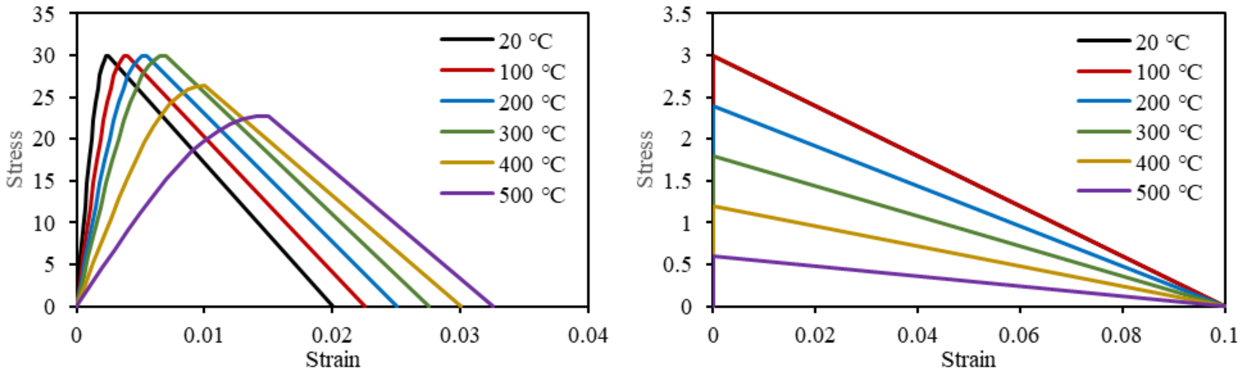

(a) Compressive stress-strain curves (b) Tensile stress-strain curves

Figure 15. Concrete material model

In compression, the stress-strain relationship given by EC2 [26] is used, in which a linear descending branch is adopted for each curve. As for concrete in tension, it is assumed that the tensile stress increases linearly with respect to strain until concrete cracking occurs, after which the stress decreases linearly to zero, and the strain corresponding to zero stress is taken as 10 times the cracking strain, as suggested by the Abaqus user's manual [30]. In this work, the tensile strength of concrete is set to be 10% of the compressive strength [31], and the total tensile strain of concrete is assumed to be 0.1 [32]. The Concrete Damage Plasticity model in Abaqus, which is suitable for materials with different tensile and compressive strengths, is adopted for concrete solid elements in this model. This material model combines the concepts of isotropic damaged elasticity and isotropic tensile and compressive plasticity to represent the inelastic behaviour of concrete. The yielded parts of the tensile and compressive stress-strain curves of concrete are entered separately into the model. The material dilation angle and eccentricity parameter are taken as 20° and 0.1, respectively. The ratio of biaxial to uniaxial compressive strength is taken as 1.16. The stress-strain relationship of carbon steel without consideration of strain-hardening specified in Eurocode

3 Part 1-2 [33] at elevated temperatures is adopted to simulate beam, column and ductile connection. This is widely used, although it is an implicit-creep model based on transient testing. The current analysis does not consider the effects of high-temperature creep explicitly.

4.2 Interaction and boundary conditions

In order to reduce the model size and to save computational cost, only a quarter of each model was built, as shown in Figure 16 (a).

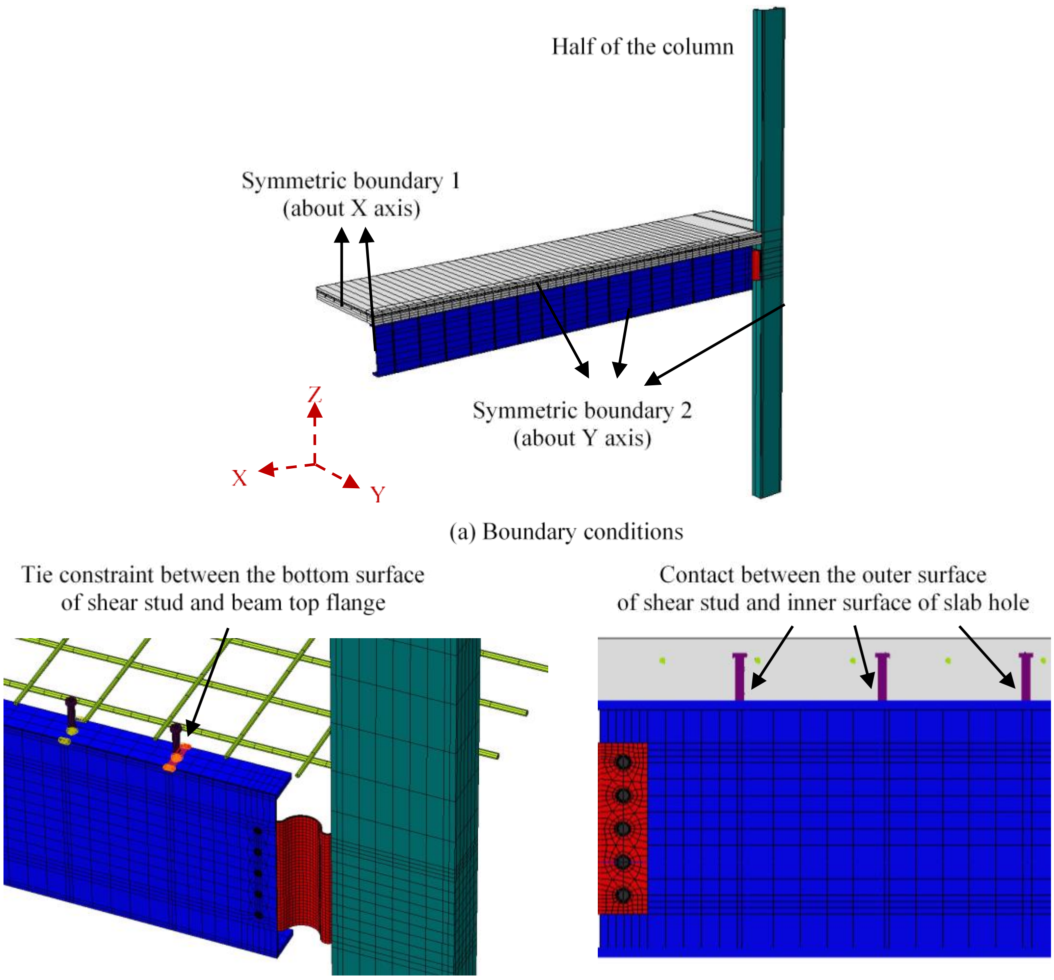

(a) Boundary conditions

(b) Method of simulating shear studs

Figure 16. The Abaqus composite frame model

The X-Z plane is assumed as a plane of symmetry throughout the model, and the Y-Z plane is assumed as a plane of symmetry at the mid-span of the composite beam. Since the purpose of these Abaqus models is to investigate the influence of shear studs on the performance of the composite ductile connection, detailed shear studs are modelled using solid elements. The bottom surface of the shear stud is tied to the steel section's top flange. A cavity is created in the slab at the position of each stud, and then hard contact between the outer surface of the stud and the inner surface of the cavity is established. Other contacts, such as contact between the slab bottom surface and steel section top flange, and those between the connection surface and beam web and the bolt shank and bolt hole, are all included in these Abaqus models. All the reinforcing bars are embedded in the slab. The slab is connected to the column using a tie constraint in the Abaqus frame model.

4.3 Validation against experiments

Limited research exists on the performance of composite connections in fire, and there is limited experimental evidence for comparison. The experiments used to validate the modelling methodology are a series of tests carried out by Al-Jabri [11]. Al-Jabri used a cruciform test arrangement with a furnace wrapping the connection zone to conduct these high-temperature experiments. His Group 5 (FLC-5) tests are selected for this validation. The experimental setup of FLC-5 consists of a pair of UKB 610x229x101 sections connected to a UKC 305x305x137 column by 10 mm thick flexible end-plates with 14 M20 Grade 8.8 bolts, as shown in Figure 17 (a). The Abaqus model is shown in Figure 17 (b).

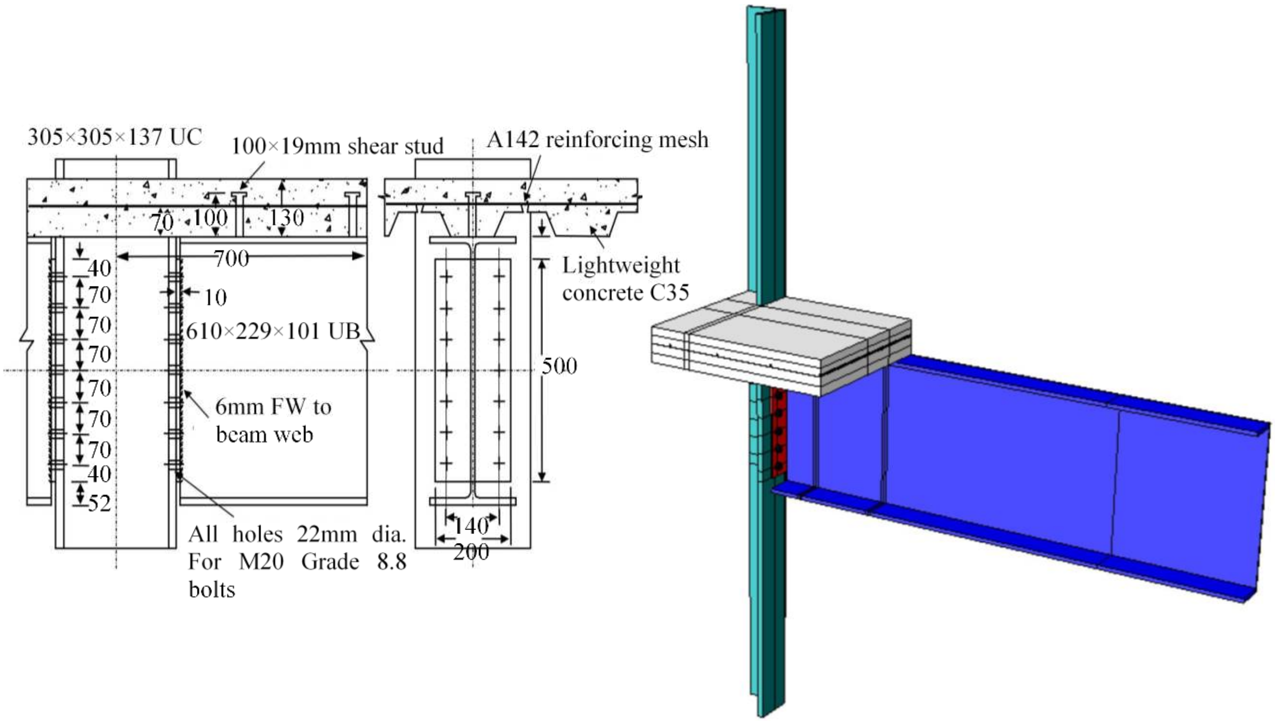

(a) Experimental setup of FLC-5[11] (b) Abaqus model

Figure 17. The Group 5 tests (FLC-5)

Two tests (FLC-5-2 and FLC-5-3) from this series were modelled. The difference between these two tests is in the applied moment. In FLC-5-2, a moment of 80 kN·m was applied at a distance of 1370 mm from the column flange surface, whereas in FLC-5-3, the applied moment increased to 134 kN·m. The comparison between the experimental results and Abaqus simulation results is shown in Figure 18. This figure shows that the overall trend of the connection rotation-beam temperature curves obtained from the experiments is very similar to those obtained from the Abaqus models. However, the temperatures at which run-away failure occurs in the experiments are lower than those of the Abaqus models. This is because, in the tests, run-away failure was caused by longitudinal splitting of the slab. This kind of cracking might cause the shear studs to separate from the slab, essentially turning the composite beam to non-composite, and eventually leading to a sudden increase in the connection rotation. Since such localised cracking is not considered in the Abaqus models, the beams in these models always remain composite. This may explain why the connection rotations of the Abaqus models are lower than those of the experiments. Other than this, the comparisons between the modelling and test results are satisfactory, validating the simulation method of the Abaqus models.

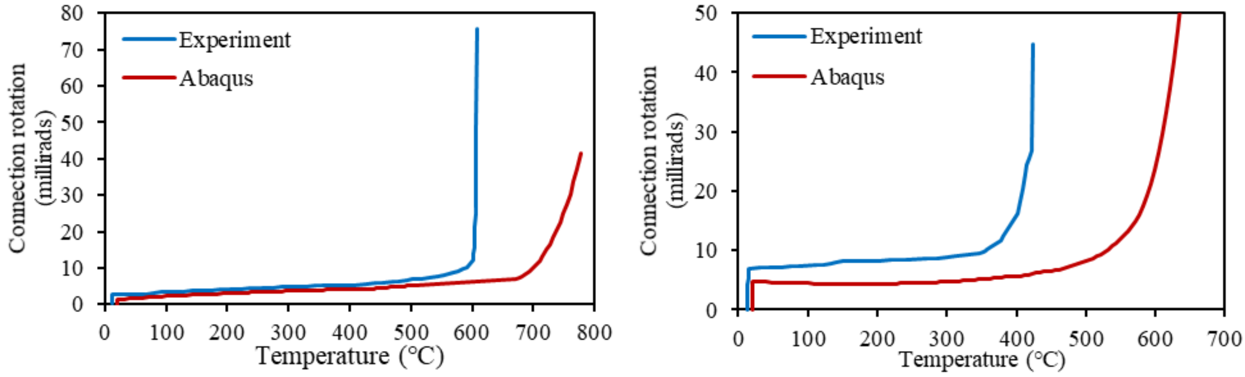

(a) FLC-5-2 (b) FLC-5-3

Figure 18. Comparison between experimental results and Abaqus results

4.4 Parametric studies using Abaqus model

In this section, the Abaqus model shown in Figure 16 (a) is used to conduct parametric studies on the influence of the shear studs on connection performance. It is assumed that the temperature of the beam bottom flange is 90% of the fire temperature, and the temperatures of beam web and top flange are 80% of the fire temperature. The lower column and the connection are protected to the same level, and their temperatures are therefore set to 50% of the fire temperature, whereas the upper column is assumed to remain at 20 °C. The temperature of the slab bottom surface is assumed to be the same as that of the beam top flange, and its top surface is assumed to remain at 20 °C throughout the analysis. The temperature distribution through slab depth is assumed to be linear.

As mentioned previously, the moment capacity of the composite beam could be reduced in cases of partial shear connection. Three different shear stud spacings are selected here, and their corresponding degrees of shear connection are listed in Table 2.

Table 2. Degrees of shear connection corresponding to different shear stud spcaings

Spacing of shear studs (mm)	Degree of shear connection
200	106.84%

500	42.74%
1000	21.37%

The comparative results for the composite frame models with different shear stud spacings are shown in Figure 19. It can be seen that the variation of stud spacing has negligible influence on the beam mid-span deflection, connection rotation, axial force in the connection and axial displacements of the top and bottom flanges of the steel section at the beam end. The only significant difference is in the beam end slip, as shown in Figure 19 (d). In this figure the slip is defined as positive when the steel section's top flange moves away from the column-face and the lower surface of the slab moves towards the column-face. If the degree of shear connection is low, the connection between the slab and steel section is weak, then they will bear the external loads more like two unconnected members. In this case, under the action of external loads at ambient temperature, the bottom surface of the slab will stretch, while the top flange of the steel section will contract, resulting in a positive beam end slip. Therefore, the composite beam with the largest stud spacing (1000 mm) experiences the largest initial positive beam end slip at ambient temperature. With increase of temperature, the steel beam expands more than concrete due to the non-uniform temperature distribution, leading to the observed change in beam end slip from positive to negative. Compared with the other two cases, the composite beam with the smallest stud spacing (200 mm) experiences the smallest negative beam end slip, because the slab provides the highest constraint to the thermal expansion of the steel beam among the three cases.

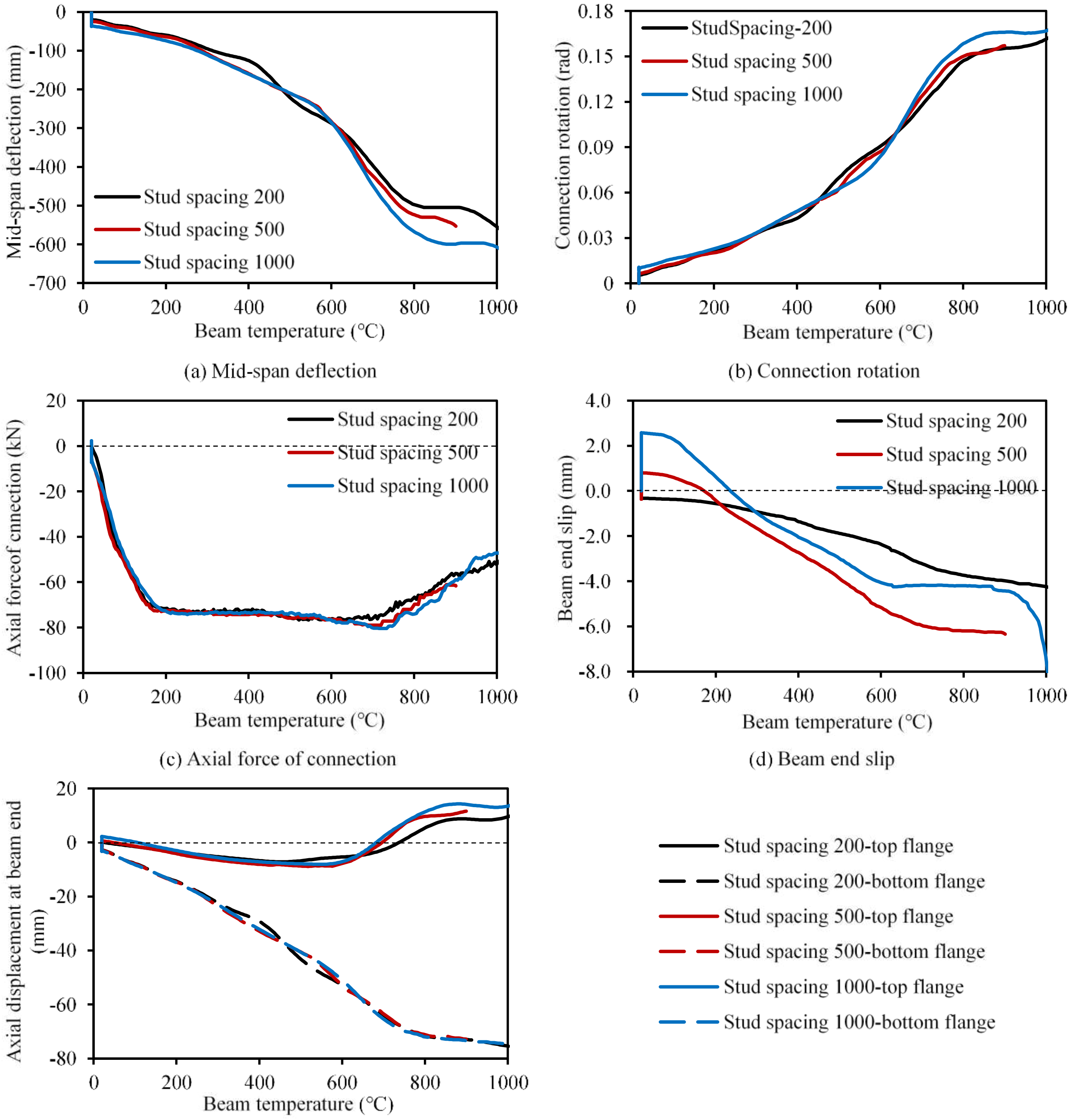

(a) Mid-span deflection

(b) Connection rotation

(c) Axial force of connection

(d) Beam end slip

(e) Axial displacement at beam end

Figure 19. Comparison of the composite frame models with different stud spacings

5. Conclusion

This paper has studied the influence of a ductile connection on the behaviour of composite beams in fire conditions. Four equations have been proposed to calculate the axial ductility demand of the composite beam at four key positions of the cross-section; the reinforcement layer, the connection top surface, the connection bottom surface, and the beam bottom flange. The deflection caused by the thermal bowing of the composite beam was included within the beam's total deflection in order to consider the effect of the concrete slab.

A component-based model of the composite ductile connection has been established by adding the reinforcement component to the bare-steel ductile connection model developed previously [18]. The proposed reinforcement component can consider the pull-out of longitudinal bars across a discrete crack above the connection, and the physical anchorages provided by the weld points to transverse bars in the welded mesh. The component-based composite ductile connection model has been converted into a connection element following the principles of the finite element method, and incorporated into the software Vulcan. A 2-D composite frame model with ductile connections has been modelled using both Vulcan and Abaqus; the latter has used a detailed model of the connection's geometry using solid elements. A comparison of the results shows that although the connection in the Abaqus model is stiffer than that in the Vulcan model, the proposed component-based composite ductile connection model can efficiently represent the behaviour of the composite ductile connection without going to the extent of creating a full model using solid elements. Parametric studies on three design parameters were carried out, including the connection thickness, the cylindrical section radius and the number of longitudinal bars in an effective width. It was found that thinner plate thickness and larger cylindrical section radii lead to higher axial ductility, which significantly reduces the axial force carried by the connection. Lower numbers of longitudinal reinforcing bars tend to lead to early failure.

Since the shear studs are not considered in the component-based composite ductile connection model, detailed Abaqus composite framed models were created to investigate the effect of shear studs on the performance of the composite ductile connection under different stud spacings. The Abaqus modelling approach was validated against the experiments previously conducted by AI-Jabri. Results show that the variation of stud spacings has little influence on the beam's mid-span deflection, connection rotation, connection axial force or the axial displacements of the top and bottom flanges of the steel section at the beam end. The only substantial difference is in the end slip between the steel section and the concrete slab. Composite beams with lower degrees of shear connection experience an initially positive end slip at ambient temperature, which becomes negative as the steel section temperature rises due to the thermal expansion.

As for future developments, it is certainly necessary to validate the analytical results experimentally, possibly using composite frames/subframes with ductile connections at reduced scale. In addition to experiments, 3-D composite frame models will be built using Vulcan, to investigate the influence of out-of-plane structure, particularly slabs, on the performance of the composite ductile connections. In practical terms, the performance of the composite ductile connections should be compared with traditional connection types, including connection types which are normally designed as "simple" in the sense that they are not assumed to transfer moments. These include the commonly-used web-cleat, fin-plate and flexible end-plate connections.

References

[1] Lennon T, Moore D, The natural fire safety concept—full-scale tests at Cardington, Fire Safety Journal, 2003;38: 623-43.
[2] Zoetemeijer P, Summary of the research on bolted beam-to-column connections, TU Delft, Faculteit der Civiele Techniek, 1990.
[3] CEN, Eurocode 3: Design of steel structures—Part 1-8: Design of joints, 2005.
[4] Wang Y-C, Composite beams with partial fire protection, Fire Safety Journal, 1998;30: 315-32.
[5] Sanad A, Rotter J, Usmani A, O'Connor M, Composite beams in large buildings under fire—numerical modelling and structural behaviour, Fire Safety Journal, 2000;35: 165-88.
[6] Foster S, Chladná M, Hsieh C, Burgess I, Plank R, Thermal and structural behaviour of a full-scale composite building subject to a severe compartment fire, Fire Safety Journal, 2007;42: 183-99.
[7] Li G-Q, Zhang N, Jiang J, Experimental investigation on thermal and mechanical behaviour of composite floors exposed to standard fire, Fire Safety Journal, 2017;89: 63-76.
[8] Wainman D, Kirby B, Compendium of UK standard fire test data: Unprotected structural steel, British Steel Corporation, Swinden Laboratories, 1988.
[9] LESTON JONES L, Jones L, BURGESS I, LENNON T, PLANK R, BRE, Elevated-temperature moment-rotation tests on steelwork connections, Proceedings of the Institution of Civil Engineers-Structures and Buildings, 1997;122: 410-19.
[10] Leston-Jones LC. The influence of semi-rigid connections on the performance of steel framed structures in fire. University of Sheffield, 1997.
[11] Al-Jabri KS. The behaviour of steel and composite beam-to-column connections in fire. University of Sheffield, 1999.
[12] Liu T, Three-dimensional modelling of steel/concrete composite connection behaviour in fire, Journal of

Constructional Steel Research, 1998;1: 319-20.
[13] Li J-T, Li G-Q, Lou G-B, Chen L-z, Experimental investigation on flush end-plate bolted composite connection in fire, Journal of Constructional Steel Research, 2012;76: 121-32.
[14] Li G-Q, Chen L-Z, Li J-T, Lou G-B, Modeling of end-plate bolted composite connection in fire considering axial force effects, Journal of Constructional Steel Research, 2012;76: 133-43.
[15] Pucinotti R, Bursi O, Franssen J-M, Lennon T, Seismic-induced fire resistance of composite welded beam-to-column joints with concrete-filled tubes, Fire Safety Journal, 2011;46: 335-47.
[16] Liu Y, Huang S-S, Burgess I, Investigation of a steel connection to accommodate ductility demand of beams in fire, Journal of Constructional Steel Research, 2019;157: 182-97.
[17] Liua Y, Huanga S-S, Burgessa I. Ductile connections to improve structural robustness in fire. In. Ductile connections to improve structural robustness in fire. Sheffield, 2019.
[18] Liu Y, Huang S-S, Burgess I, Component-based modelling of a novel ductile steel connection, Engineering Structures, 2020;208: 110320.
[19] Liu Y, Huang S-S, Burgess I, Performance of a novel ductile connection in steel-framed structures under fire conditions, Journal of Constructional Steel Research, 2020;169: 106034.
[20] Madas PJ, Advanced modelling of composite frames subject to earthquake loading, 1993.
[21] Rassati G, Leon RT, Noè S, Component modeling of partially restrained composite joints under cyclic and dynamic loading, Journal of Structural Engineering, 2004;130: 343-51.
[22] Sezen H, Setzler EJ, Reinforcement slip in reinforced concrete columns, ACI Structural Journal, 2008;105: 280.
[23] Sezen H, Seismic behavior and modeling of reinforced concrete building columns, 2004.
[24] Lynn A, Moehle J, Seismic evaluation of existing reinforced concrete, Journal of Prestressed concrete Institute, 1996;17.
[25] Burgess I, Sahin M. Tensile Membrane Action of Lightly-reinforced Rectangular Composite Slabs in Fire. In. Tensile Membrane Action of Lightly-reinforced Rectangular Composite Slabs in Fire. Elsevier, 2018, pp. 176-97.
[26] En B, 1-2: 2004 Eurocode 2: Design of concrete structures-Part 1-2: General rules-Structural fire design, European Standards, London, 2004.
[27] Lawson R, Behaviour of steel beam-to-column connections in fire, Structural engineer, 1990;68: 263-71.
[28] Lawson R, Enhancement of fire resistance of beams by beam to column connections, Steel Construction Institute UK, 1990.
[29] Institution BS, Eurocode 2: Design of concrete structures: Part 1-1: General rules and rules for buildings, British Standards Institution, 2004.
[30] Hibbett, Karlsson, Sorensen, ABAQUS/standard: User's Manual, Hibbitt, Karlsson & Sorensen, 1998.
[31] Pi Y-L, Bradford MA, Uy B, Second order nonlinear inelastic analysis of composite steel–concrete members. I: Theory, Journal of Structural Engineering, 2006;132: 751-61.
[32] Liang QQ, Uy B, Bradford MA, Ronagh HR, Strength analysis of steel–concrete composite beams in combined bending and shear, Journal of Structural Engineering, 2005;131: 1593-600.
[33] CEN. Eurocode 3: Design of steel structures, Part 1–2: General rules—Structural fire design. BS EN 1993-1-2: 2005. In. Eurocode 3: Design of steel structures, Part 1–2: General rules—Structural fire design. BS EN 1993-1-2: 2005. 2005.